Published in final edited form as:
Mater Today (Kidlington). 2019 May 29; 30: 10–16. doi:10.1016/j.mattod.2019.04.002.

Stable and optoelectronic dipeptide assemblies for power harvesting

Kai Tao[#1], **Bin Xue**[#2], **Qi Li**[#3,4], **Wen Hu**[5], **Linda J.W. Shimon**[6], **Pandeeswar Makam**[1], **Mingsu Si**[7], **Xuehai Yan**[8], **Mingjun Zhang**[9], **Yi Cao**[2], **Rusen Yang**[5,*], **Junbai Li**[3,4,*], **Ehud Gazit**[1,10,*]

[1]Department of Molecular Microbiology and Biotechnology, George S. Wise Faculty of Life Sciences, Tel Aviv University, Tel Aviv 6997801, Israel

[2]Collaborative Innovation Centre of Advanced Microstructures, National Laboratory of Solid State Microstructure, Department of Physics, Nanjing University, 22 Hankou Road, Nanjing 210093, Jiangsu, China

[3]Beijing National Laboratory for Molecular Sciences, CAS Key Lab of Colloid, Interface and Chemical Thermodynamics, Institute of Chemistry, Chinese Academy of Sciences, Beijing 100190, China

[4]National Centre for Nanoscience and Technology, Beijing 100190, China

[5]School of Advanced Materials and Nanotechnology, Xidian University, Xi'an 710126, China

[6]Department of Chemical Research Support, Weizmann Institute of Science, Rehovot 7610001, Israel

[7]Key Laboratory for Magnetism and Magnetic Materials of the Ministry of Education, Lanzhou University, Lanzhou 730000, China

[8]State Key Laboratory of Biochemical Engineering, Institute of Process Engineering, Chinese Academy of Sciences, Beijing 100190, China

[9]Department of Biomedical Engineering, College of Engineering, The Ohio State University, Columbus, OH 43210, USA

[10]Department of Materials Science and Engineering, Iby and Aladar Fleischman Faculty of Engineering, Tel Aviv University, Tel Aviv 6997801, Israel

[#] These authors contributed equally to this work.

Abstract

[*]Corresponding authors. Yang, R. (rsyang@xidian.edu.cn), Li, J. (jbli@iccas.ac.cn), Gazit, E. (ehudg@post.tau.ac.il).

Author contributions

R.S.Y., J.B.L., and E.G. conceived and designed the work; K.T. and P.M. conducted crystal growth, SEM, TGA, fluorescence and FLIM characterizations; B.X. and Y.C. conducted experimental measurements of mechanical properties; Q.L., X.H.Y., and J.B. L. performed the optical waveguiding experiment; W.H. and R. S.Y. fabricated the power generator and characterized its performances; M.S.S. performed DFT calculations of band structures and partial density of states of crystals; K.T. and L.J.W.S. performed crystallography analysis. K.T., B.X., and Q.L. coordinated all the work, analyzed the results, and wrote and edited the manuscript with input from all authors.

Competing interests

The authors declare no competing interests.

Europe PMC Funders Author Manuscripts

Low biocompatibility or engineerability of conventional inorganic materials limits their extensive application for power harvesting in biological systems or at bio-machine interfaces. In contrast, intrinsically biocompatible peptide self-assemblies have shown promising potential as a new type of ideal components for eco-friendly optoelectronic energy-harvesting devices. However, the structural instability, weak mechanical strength, and inefficient optical or electrical properties severely impede their extensive application. Here, we demonstrate tryptophan-based aromatic dipeptide supramolecular structures to be direct wide-gap semiconductors. The molecular packings can be effectively modulated by changing the peptide sequence. The extensive and directional hydrogen bonding and aromatic interactions endow the structures with unique rigidity and thermal stability, as well as a wide-spectrum photoluminescence covering nearly the entire visible region, optical waveguiding, temperature/irradiation-dependent conductivity, and the ability to sustain quite high external electric fields. Furthermore, the assemblies display high piezoelectric properties, with a measured open-circuit voltage of up to 1.4 V. Our work provides insights into using aromatic short peptide self-assemblies for the fabrication of biocompatible, miniaturized electronics for power generation with tailored semiconducting optoelectronic properties and improved structural stability.

Introduction

Organic semiconductors are ideal constituents for next-generation optoelectronic microdevices owing to their diverse and tuneable properties, cost effectiveness, and ease of modulation [1,2]. However, the design of a simple system simultaneously presenting high mechanical rigidity, similar to inorganic components, and stable optoelectronic properties in the visible region for power generation is still to be demonstrated, thus currently hindering their applications for high-integrated bio-electronic devices and at the interface with complicated biological systems [3,4]. Therefore, there is an ongoing search for alternatives that would provide enhanced eco-friendliness and ease of tunability, along with other required properties, including strong structural rigidity, flexible morphology modulation, and efficient optical or electronic behaviors [5,6].

Several natural polypeptide and protein self-assemblies have been recently found to show intrinsic semiconductive properties [7], resulting from hydrogen bonding networks among peptide backbones [8] or π–π interactions between side-chain aromatic moieties [9]. Inspired by nature, aromatic dipeptide self-assemblies, incorporating hydrogen bonding and aromatic interactions, may be promising candidates to overcome these challenges [10–13]. Specifically, tryptophan (W)-based aromatic dipeptide self-assemblies are expected to integrate and enhance diverse physicochemical properties in a single system due to the additional hydrogen bonding and aromatic interactions mediated by the side-chain heterocyclic indole ring [14]. However, the design of simple W-based peptide self-assembling platforms simultaneously presenting high mechanical rigidity and broad optoelectronic properties for power generation is still to be demonstrated [15].

Here, to thoroughly explore their potentially applicable properties, we designed and crystallized W-containing aromatic dipeptides, both linear and cyclic (Table S1 in the supporting material); validated their supramolecular structures; and comprehensively

characterized their unique mechanical, optoelectronic, and piezoelectric features. Our results demonstrate that the aromatic dipeptide crystal packings may be used as a new type of bio-organic semiconductors for fabrication of energy harvesting microdevices that combine high structural stability with tailored optoelectronics.

Results and discussion

Crystallographic analysis showed the examined W-based dipeptides crystalized into monoclinic or orthorhombic structures (Table S1 and cif. files in the supporting material), thus presenting high aspect-ratio, needle-like morphologies (Fig. 1a). The diverse peptide sequences gave rise to various supramolecular frameworks with different hydrogen bonding and π–π interaction networks [16]. In cyclo-phenylalanine–tryptophan (cyclo-FW) and cyclo-tryptophan–tryptophan (cyclo-WW) crystals (Fig. 1a), the backbone diketopiperazine rings were parallelly organized by hydrogen bonding, with $N(H)_{backbone}\cdots O{=}C$ (donor⋯acceptor) distances of 2.88 Å or 2.97 Å and 2.93 Å, respectively (Fig. 1b, c, “1”). Intriguingly, water molecules played crucial roles in crystallization of the aromatic dipeptides. Specifically, in the cyclo-FW crystal, the monomers were connected from one backbone diketopiperazine ring to another side-chain indole ring through a water molecule by forming a hydrogen bond with an $O(H)_{water}\cdots O{=}C$ distance of 2.79 Å and $N(H)_{indole}\cdots O_{water}$ distance of 2.86 Å (Fig. 1b, “2”). In the cyclo-WW crystals, adjacent backbone diketopiperazine rings were linked through two pairs of water molecules, each forming three hydrogen bonds with two $O(H)_{water}\cdots O{=}C$ and one $O(H)_{water}\cdots O_{water}$ distances of 2.80 Å, 2.73 Å, and 2.81 Å, respectively (Fig. 1c, “3”). Thus, a quasi-rectangular, hydrophilic channel was formed, connected to the side-chain indole rings through a water molecule on each side by forming two hydrogen bonds with $O(H)_{water}\cdots O_{water}$ and $N(H)_{indole}\cdots O_{water}$ distances of 2.74 Å and 2.86 Å, respectively (Fig. 1c, “3”). The channels were 235 $Å^3$ in size and comprised ~11% of the unit cell volume, thus exemplifying the microporous nature of the cyclo-WW crystals.

In addition to the hydrogen-bonding interface, the aromatic side-chains were organized into hydrophobic π-electron delocalized domains. In both the cyclo-FW and the cyclo-WW crystals, the hydrophobic domains were composed of four side-chains. Specifically, in the cyclo-FW system, the dominant aromatic interactions were of “parallel displayed” mode (Fig. 1b, “3”). The dihedral angles between phenyl rings or between phenyl and indole rings were both 34°, with nearest inter-atom distances of 3.6 Å and 3.8 Å, respectively (Fig. 1b, “3”). In contrast, the cyclo-WW system exhibited the “edge-to-face” mode as the main aromatic interaction, with a dihedral angle of 61° between the indole rings and a nearest inter-atom distance of 3.6 Å (Fig. 1c, “2”).

The notable difference between the structures demonstrates that the peptide supramolecular structures, along with their macroscopic properties, can be tuned by modifying the peptide sequence [17]. Particularly, the number of water molecules per peptide monomer in the crystal could be finely modulated, ranging from zero (cyclo-FF [18], cyclo-GW), one (cyclo-FW, cyclo-W (*d*)W; the italic *d* represents *D*-type amino acid), two (linear-FF [19], linear-GW), three (cyclo-WW) to even four water molecules (linear-W(*d*)W) (Fig. 1d, Fig. S1 in the supporting material). Recent studies demonstrated that the water molecules play

important roles in the electronic properties of peptide selfassemblies [20,21] by influencing the hydrogen bonding interactions [22]. Therefore, the diverse numbers of water molecules in the dipeptide crystals imply their distinct structure-encoded physicochemical behaviors. Correspondingly, the crystals could be categorized into several groups (Fig. 1, Fig. S1 in the supporting material): (i) Crystals forming alternating hydrophilic-hydrophobic architectures (cyclo-FF, linear-GW, cyclo-GW and cyclo-W(*d*)W; Fig. S1 in the supporting material). (ii) Crystals composed of interval hydrophilic and hydrophobic regions (cyclo-FW; Fig. 1c, Fig. S1e in the supporting material). (iii) Crystals comprising internal channels, with the cavity nature depending on the amino acid residues [23]. Thus, circular (linear-FF, Fig. S1a in the supporting material) or rectangular (cyclo-WW, Fig. 1c, Fig. S1f in the supporting material) channels could be designed. The porous nature suggests the potential of the dipeptide crystals to serve as supramolecular microporous frameworks, thereby supplementing the state-of-the-art inorganic (such as zeolite) and hybrid (such as metal organic frameworks) counterparts [24]. On the other hand, the linear-W(*d*)W crystals contained a layer of water molecule network entrapped between two layers of peptide molecules (Fig. S1g in the supporting material). This sandwich structure could confer properties of proton-based conductivity and transfer.

The extensive and directional hydrogen bonding and aromatic interactions suggest that the supramolecular arrangement can exhibit high structural stability and mechanical strength [25]. At the macroscopic level, thermal gravimetric analysis (TGA) characterizations demonstrated that the cyclo-FW crystals could sustain up to 370 °C (Fig. 2a, red curve). Notably, the cyclo-FF crystals started to degrade at 303 °C (Fig. 2a, black curve), implying that W-based dipeptide crystals are more stable than F-based ones. This is probably due to the contribution of more hydrogen bonding and aromatic interactions supplied by the side-chain indole rings. As controls, the well-characterized linear dipeptides (linear-FF, linear-FW) showed a loss of a water molecule from every monomer and their crystals transformed into the cyclic counterparts (cyclo-FF, cyclo-FW, respectively) at 170 °C (Fig. 2a, marked by arrow) [15,26]. The high thermal stability of the cyclic dipeptides suggests their potential use in a wide temperature range under heat losses in working microdevices [15,27].

The remarkable thermal resistance suggests that the crystals may possess high mechanical strength at the microscopic level as well. Nano-indentation through atomic force microscopy (AFM) was used to experimentally validate the micromechanical properties of the crystals. The elasticity of the crystals showed Young's modulus of 17.4 ± 5.8 GPa (Fig. 2b), significantly higher than that of dragline silk (10 GPa) [28], insulin self-assembling nanofibers (3.3 ± 0.4 GPa) [29], and Tobacco Mosaic Virus self-assembling nanotubes (0.9 ± 0.2 GPa) [30], with an average point stiffness of 5.38 N m^{-1} (Fig. 2c), a high value for biological components. Correspondingly, the shear modulus perpendicular to the crystal axis direction was measured to be 0.2 ± 0.14 GPa (Fig. 2d), similar to the well-characterized rigid FF nanotubes (0.21 ± 0.03 GPa) [31]. These findings reveal that the cyclo-FW crystals present significant mechanical stability, thus bearing the potential to serve as bio-inspired components for micromechanical applications [15,32].

The hydrogen bonding and aromatic interaction networks can decrease the bandgap between the lowest unoccupied and the highest occupied molecular orbitals [33,34]. Computational

density functional theory calculations showed the bandgap of cyclo-FW crystals to be approximately 3.1 eV (Fig. 3a). The corresponding band structure is displayed in Fig. 3b, showing that the highest occupied band below the Fermi level was completely localized in the first Brillouin zone. In contrast, the lowest unoccupied state appeared at the G point and was slightly dispersed. This demonstrates that the cyclo-FW crystals are direct wide-gap semiconductors with inter-band transition at the G point [35]. Furthermore, when replacing F with W, the introduction of more hydrogen bonding and aromatic interaction led to a lower bandgap of 2.8 eV for the cyclo-WW crystals (Fig. S2 in the supporting material). Fluorescent characterization of the cyclo-FW crystals demonstrated emission ranging from 395 nm to 550 nm, a wide-spectrum in the visible light region, when excited at 300–500 nm (Fig. 3c, *i*). A similar emission could also be detected for cyclo-WW and cyclo-W(*d*)W crystals, namely 485–560 nm (Fig. 3c, *ii*) and 400–600 nm (Fig. 3c, *iii*), respectively. The multicomponent spectrum of cyclo-FW, comprising a dominant peak at 395 nm and a satellite peak at 440 nm upon excitation at 300 nm, compared with the smooth, single-peak curves of cyclo-WW and cyclo-W(*d*)W (Fig. 3c, black curves), demonstrates that the intrinsic emission of the amino acid residues existed in the cyclo-FW fluorescence profile. In addition, both linear-FF and cyclo-FF presented a constant emission regardless of the excitation wavelength (Fig. S3 in the supporting material). These findings illustrate the more efficient self-assembly into supramolecular semiconductors of W-containing peptides, as compared to F [14–16]. Fluorescent microscopy investigations confirmed the photoluminescence feature of the crystals, showing altered colours of emission from blue to red under different excitation wavelengths (Fig. S4 in the supporting material). Fluorescence lifetime microscopy (FLIM) analysis revealed that the fluorescence lifetime of the crystals was very short, only 0.8 ns for cyclo-FW, 1.4 ns for cyclo-WW and 1.5 ns for cyclo-W(*d*)W crystals (Fig. 3d, Fig. S5 in the supporting material), compared with 2.1 ns for the less photoactive cyclo-GW crystals [15]. Notably, the photoluminescence abruptly attenuated under continuous excitation (Fig. 3e), rather than keeping constant as shown for cyclo-GW [15], indicating that the photons could easily transfer along the crystals [36]. Therefore, when focusing the excitation at the bulky region of the cyclo-FW crystals in a custom-designed optical waveguide measurement setup (Fig. S6 in the supporting material), the emission light could be shown to come out from the terminals (Fig. 3f). Furthermore, the intensity of the emission output could be finely tuned by controlling the excitation position or intensity (blue and red circles in Fig. 3f). We propose that after packing, the restriction of molecular motions by the non-covalent interactions, such as molecular rotations or vibrations, impeded the energy dissipation and led to the constant photon emission [37]. This demonstrates the potential of the peptide crystals as optical components for microscale devices, such as optical waveguiding [38].

In contrast to regular conductors, semiconductors typically show enhanced conductivity upon temperature increase [39]. By casting cyclo-FW crystals on an Au electrode (Fig. 4a, inset) with a custom-designed photoelectric test platform (Fig. S7 in the supporting material), temperature-controlled conductivity could be characterized, as shown in Fig. 4a. Notably, the resistance showed a sharp decline from 5.2 TΩ to 2.3 TΩ as the temperature increased from 340 K to 400 K (Fig. 4b, Fig. S8 in the supporting material), with an apparent large slope of −48.5 GΩ K^{-1}. Considering that the excited electrons can be easily

transferred along the crystals, the conductivity of the crystals can be enhanced through light irradiation. Specifically, an around 3 mm-long cyclo-FW crystal showed a high resistance of 0.9 TΩ in the dark, as measured by fixing the tungsten needle electrodes at the two ends (Fig. 4c, inset), which significantly decreased by 67% to 0.3 TΩunder UV illumination (256 nm) (Fig. 4c). These thermo- and opto-stimulated electrical analyses suggest a broad application potential of the peptide semiconductors, such as for solar cells [40]. Furthermore, the rigid nature of the crystals conferred these organic materials high stability against external voltages. Thus, another around 1 mm-long cyclo-FW crystal was found to retain constant resistance in an external electric field of up to 120 kV m^{-1} and broke down only when the field intensity increased to more than 166 kV m^{-1}, implying that at these values, the electric field could destroy the hydrogen bonding and aromatic interaction networks, thus resulting in a distinct increase of the resistance (Fig. 4d).

These notable mechanical, optical and electrical features endow the peptide crystals the ability to be used for bioorganic electronics [41–43]. Given the non-centrosymmetric nature of the cyclo-FW crystals (Table S1 in the supporting material), we designed and fabricated a minimized power generator using their piezoelectric properties, as shown in Fig. 4e. Briefly, the cyclo-FW crystals were sandwiched between two Ag-coated silicon substrates connected to an external measuring instrument (Fig. 4f). When a periodic compressive force of 56 N was applied to the power generator, the output open-circuit voltage (V_{oc}) after offset calibration reached up to 1.4 V (Fig. 4g). This voltage is similar to that of FF microrod arrays (1.4 V) [13] and significantly higher than that of glycine crystals (0.45 V) [44] and M13 bacteriophage (0.4 V) [45] based bioinspired piezoelectric power generators. Correspondingly, the short-circuit current (I_{sc}) reached 1.75 nA (Fig. 4h). Switching-connection tests revealed that the opposite output signals were achieved when the connection to the measurement instrument was reversed (Fig. S9 in the supporting material). This excluded the possible errors from the variation of contact resistance or parasitic capacitance and confirmed that the detected electrical signal indeed emanated from the piezoelectric cyclo-FW crystals. Furthermore, the V_{oc} values were proportional to the applied forces, with a slope of 28 mV N^{-1} (Fig. 4i), thus demonstrating the linear piezoelectricity of the peptide crystals.

Conclusions

In summary, we demonstrate the W-based aromatic dipeptide crystal packings examined here to be direct wide-gap semiconductors. The extensive and directional hydrogen bonding and aromatic interactions endow these structures with high micromechanical toughness and thermal stability, wide-spectrum visible photoluminescence, and notable optical waveguiding behaviors, along with thermo- and opto-modulated conductivity. Especially, the crystals show a significant piezoelectric effect, allowing the generation of high, stable power outputs under high pressing forces in proof-of-concept devices. Furthermore, the crystal structures can be easily tuned through modulation of the molecular sequences, thereby adjusting their physiochemical features and functionalities. Given their intrinsic advantages of eco-friendliness, inherent bioavailability, morphological and functional flexibility, and ease of fabrication, these peptide self-assemblies may serve as bio-organic, supramolecular semiconductors to fabricate biocompatible microelectronics for power generation (such as

biomechanical energy harvesting) or sensing (such as heartbeat detection), with tailored optoelectronic properties and improved mechanical stability.

Supplementary Material

Refer to Web version on PubMed Central for supplementary material.

Acknowledgments

This work was supported in part by the European Research Council under the European Union Horizon 2020 research and innovation program (no. 694426) (E.G.), Huawei Technologies Co., Ltd. (E.G.), National Natural Science Foundation of China (No. 21433010, 21320102004) (J.B.L.), (No. 11804148) (B.X.). The authors thank Prof. Leeor Kronik, Dr. Samuel Frere, Mr. Noam Brown, Dr. Ido Azuri, Dr. Yong Qin, Dr. Long Gu, and Ms. Ruth Aizen for experimental and computational assistance; Dr. Sigal Rencus-Lazar for language editing; and the members of the Yang, Li, and Gazit laboratories for helpful discussions.

References

[1]. Sytnyk M, et al. Nat Commun. 2017; 8:91. [PubMed: 28733618]
[2]. Takimiya K, et al. Acc Chem Res. 2014; 47:1493–1502. [PubMed: 24785263]
[3]. Aida T, Meijer EW, Stupp SI. Science. 2012; 335:813–817. [PubMed: 22344437]
[4]. Tao K, et al. Science. 2017; 358:eaam9756. [PubMed: 29146781]
[5]. Hauser CAE, Zhang SG. Nature. 2010; 468:516–517. [PubMed: 21107418]
[6]. Gazit E. Nat Nanotechnol. 2016; 11:309–310. [PubMed: 26751168]
[7]. Pinotsi D, et al. ChemBioChem. 2013; 14:846–850. [PubMed: 23592254]
[8]. Pinotsi D, et al. J Am Chem Soc. 2016; 138:3046–3057. [PubMed: 26824778]
[9]. Amdursky N, et al. J Am Chem Soc. 2010; 132:15632–15636. [PubMed: 20958029]
[10]. Levin A, et al. Nat Phys. 2016; 12:926–930.
[11]. Fan Z, et al. Nat Nanotechnol. 2016; 11:388–394. [PubMed: 26751169]
[12]. Lee JS, et al. Angew Chem Int Ed. 2011; 50:1164–1167.
[13]. Nguyen V, et al. Commun. 2016; 7:13566.
[14]. Tao K, et al. Nat Commun. 2018; 9:3217. [PubMed: 30104564]
[15]. Tao K, et al. Adv Mater. 2019; 31
[16]. Akdim B, Pachter R, Naik RR. Appl Phys Lett. 2015; 106:183707.
[17]. Lampel A, et al. Science. 2017; 356:1064–1068. [PubMed: 28596363]
[18]. Arnon ZA, et al. Nat Commun. 2016; 7:13190. [PubMed: 27779182]
[19]. Görbitz CH. Chem Commun. 2006:2332–2334.
[20]. Görbitz CH. Chem Eur J. 2001; 7:5153–5159. [PubMed: 11775688]
[21]. Amit M, et al. Adv Funct Mater. 2014; 24:5873–5880.
[22]. Esin A, et al. Appl Phys Lett. 2016; 109
[23]. Görbitz CH. Chem Eur J. 2007; 13:1022–1031. [PubMed: 17200919]
[24]. Bracco S, et al. Chem Commun. 2018; 54:148–151.
[25]. Azuri I, et al. J Am Chem Soc. 2014; 136:963–969. [PubMed: 24368025]
[26]. Adler-Abramovich L, et al. Nat Nanotechnol. 2009; 4:849–854. [PubMed: 19893524]
[27]. Majumdar A. Science. 2004; 303:777–778. [PubMed: 14764859]
[28]. Knowles TP, et al. Science. 2007; 318:1900–1903. [PubMed: 18096801]
[29]. Smith JF, et al. PNAS. 2006; 103:5806–15811.
[30]. Zhao Y, Ge Z, Fang J. Phys Rev E. 2008; 78
[31]. Niu LJ, et al. Langmuir. 2007; 23:7443–7446. [PubMed: 17550276]
[32]. Knowles TPJ, Buehler MJ. Nat Nanotechnol. 2011; 6:469–479. [PubMed: 21804553]

[33]. Głowacki ED, et al. Org Electron. 2014; 15:3521–3528. [PubMed: 25642158]
[34]. Zhang HK, et al. J Am Chem Soc. 2017; 139:16264–16272. [PubMed: 29064249]
[35]. Maia FF Jr, et al. J Chem Phys. 2011; 134:175101. [PubMed: 21548706]
[36]. Tao K, et al. Chem Mater. 2017; 29:4454–4460. [PubMed: 28572704]
[37]. Mei J, et al. Adv Mater. 2014; 26:5429–5479. [PubMed: 24975272]
[38]. Li Q, et al. ACS Nano. 2015; 9:2689–2695. [PubMed: 25759013]
[39]. Esaki L, Tsu R. IBM J Res Dev. 1970; 14:61–65.
[40]. Ma YL, Kang ZJ, Zheng QD. J Mater Chem. 2017; A 5:1860–1872.
[41]. Nanthakumar SS, et al. J Mech Phys Solids. 2017; 105:217–234.
[42]. Nguyen BH, Zhuang X, Rabczuk T. Comput Methods Appl Mech Energy. 2019; 346:1074–1095.
[43]. Do, Hien V; , et al. Comput Struct. 2019; 214:1–14.
[44]. Guerin S, et al. Nat Mater. 2018; 17:180–186. [PubMed: 29200197]
[45]. Lee BY, et al. Nat Nanotechnol. 2012; 7:351–356. [PubMed: 22581406]

Europe PMC Funders Author Manuscripts

Europe PMC Funders Author Manuscripts

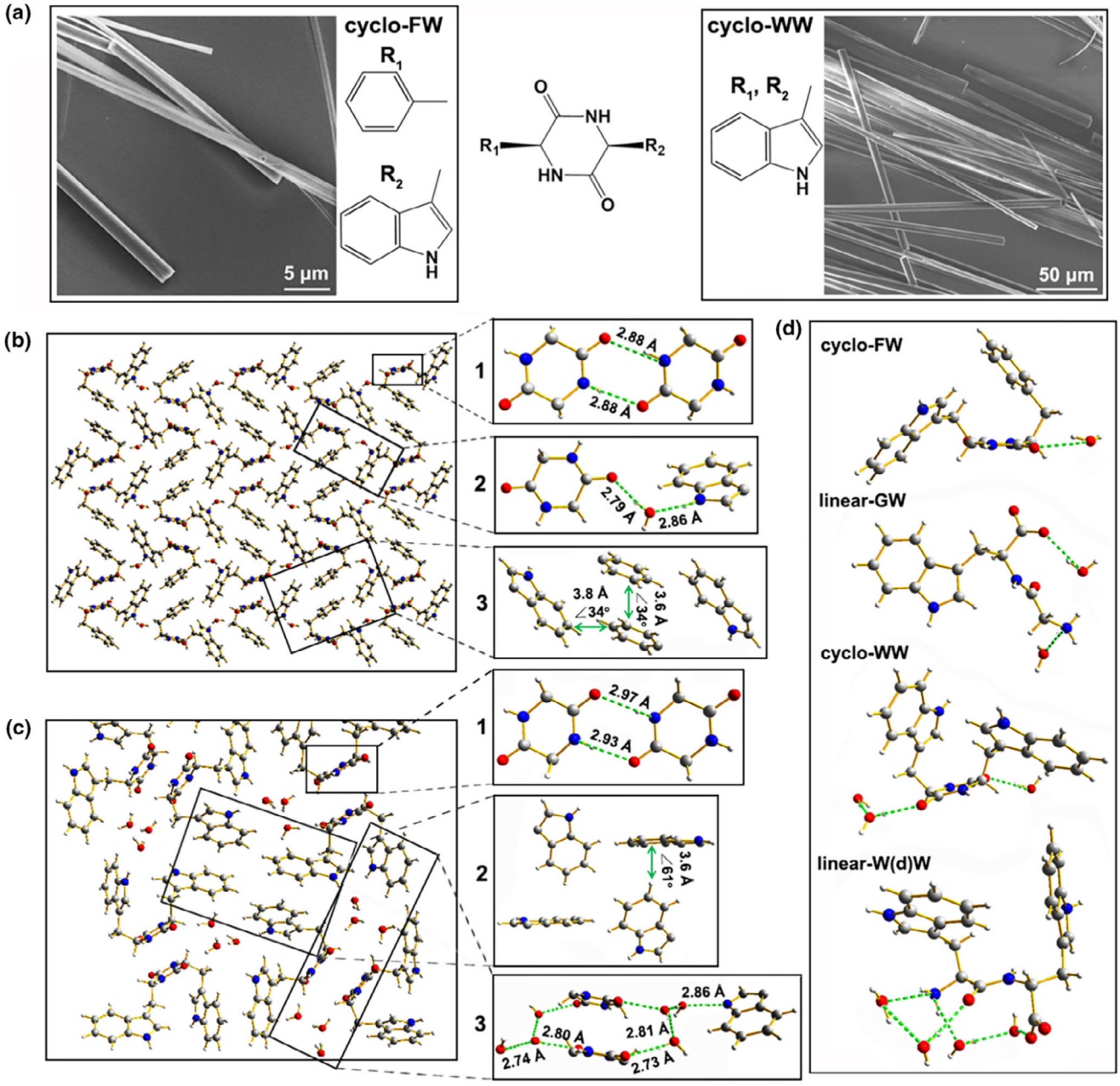

Figure 1. Crystal structures of the aromatic dipeptide packings.

(a) Molecular structures and the corresponding crystal morphologies of cyclo-FW (left) and cyclo-WW (right). (b) Crystallographic structure of cyclo-FW. The hydrogen bonding between backbone diketopiperazine rings, the water bridge, and the hydrophobic zone composed of side-chain aromatic moieties are magnified in the right panels and marked as “1”, “2”, and “3”, respectively. (c) Crystallographic structure of cyclo-WW. The hydrogen bonding between backbone diketopiperazines, the hydrophobic zone composed of side-chain aromatic moieties, and the water bridged hydrophilic channels are magnified in the right panels and marked as “1”, “2”, and “3”, respectively. (d) Monomeric crystal structures of W-

containing dipeptides: cyclo-FW, linear-GW, cyclo-WW, and linear-W(*d*)W. The monomers incorporate a different number of water molecules, ranging from one to four, respectively. Note that in (b–d) the hydrogen bonds are labeled between the donor and acceptor atoms.

Europe PMC Funders Author Manuscripts

Europe PMC Funders Author Manuscripts

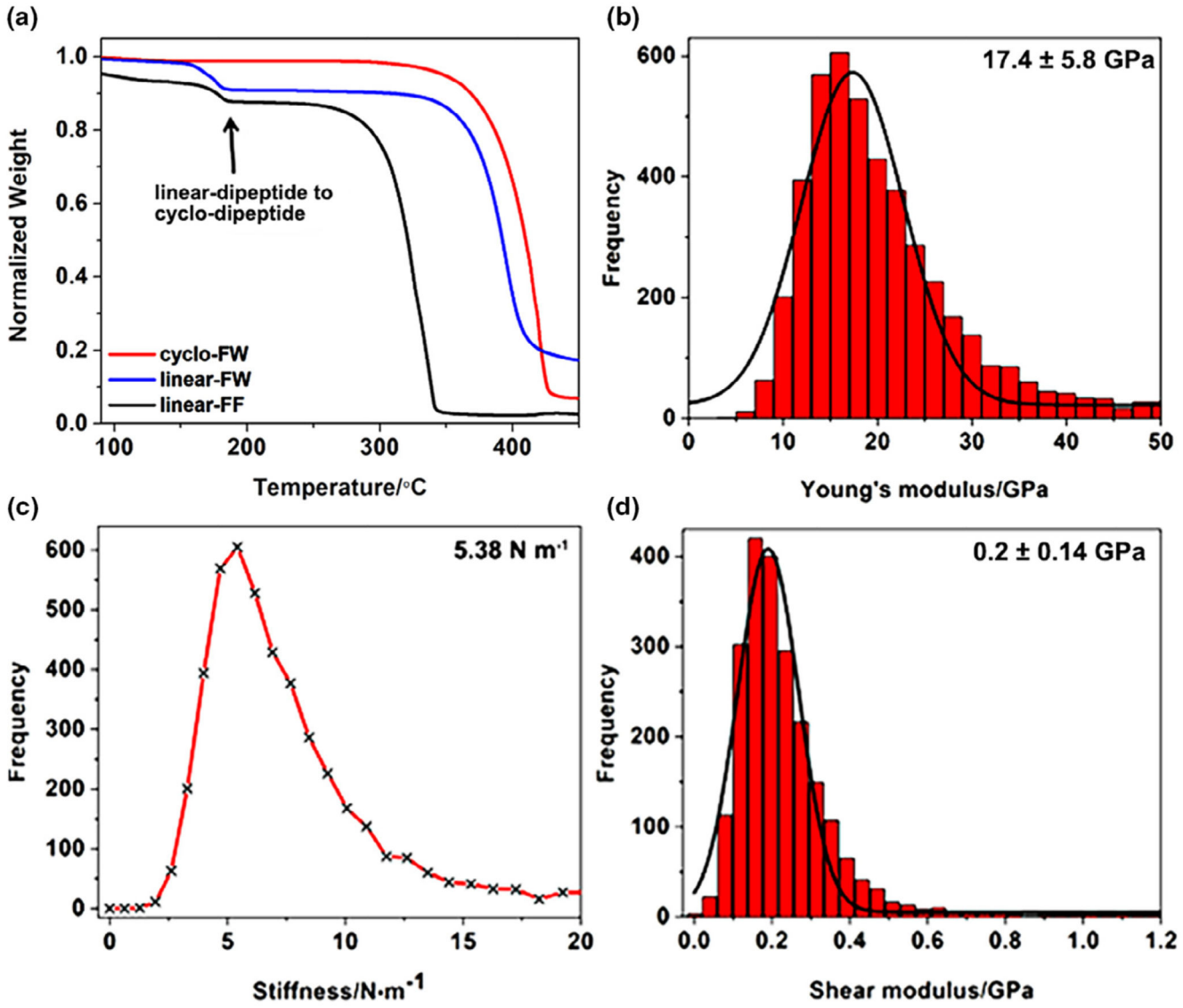

Figure 2. Mechanical properties of the aromatic cyclo-dipeptide crystals.

(a) TGA curves of the dipeptide crystals. Note that at 170 °C (marked by arrow), linear-dipeptides transform into the cyclic counterparts due to intramolecular concentration following the removal of a water molecule. (b–d) Statistical distributions of (b) Young's modulus, (c) Point stiffness, and (d) Shear modulus of the cyclo-FW crystals.

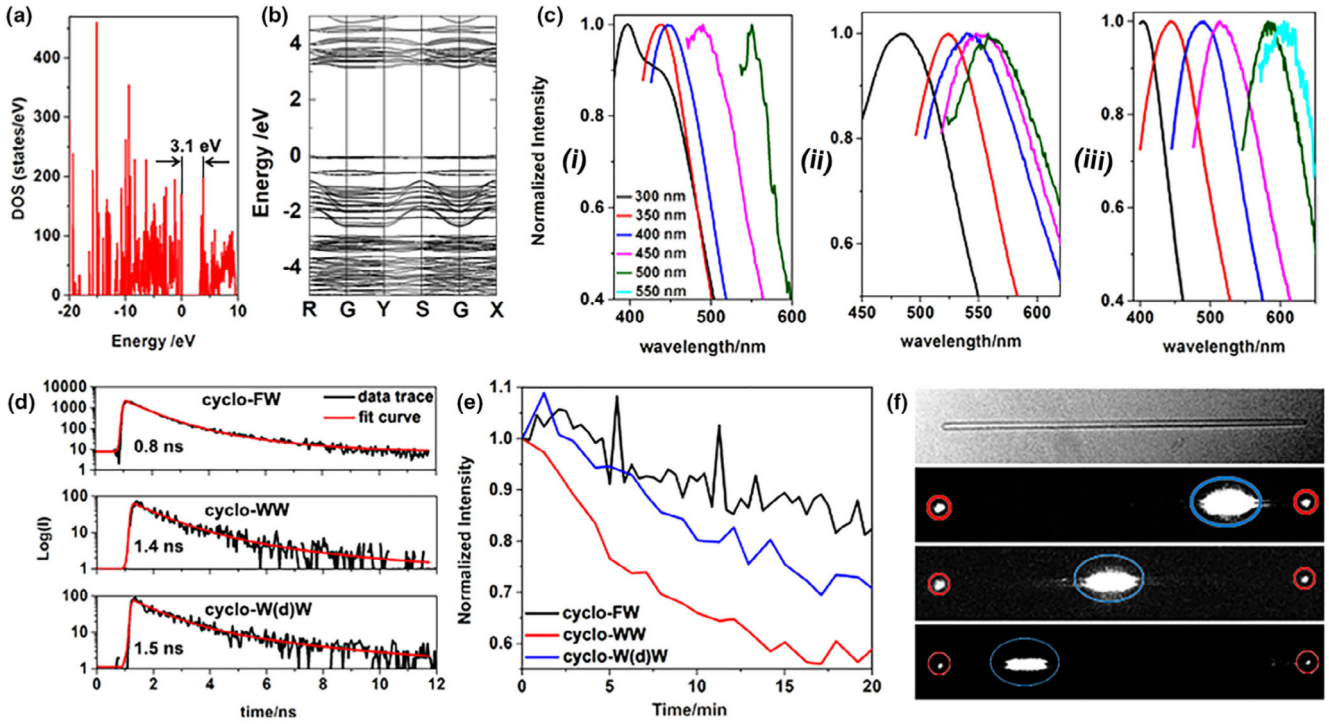

Figure 3. Photoluminescent properties of the cyclo-dipeptide crystals.

(a) Calculated bandgaps of cyclo-FW crystals. (b) Close-ups of the electronic band structures of cyclo-FW crystals near their main band gaps. Direct electron transitions occur at the G point. (c) Fluorescent emission spectra under different excitation wavelengths: *i*, cyclo-FW; *ii*, cyclo-WW; *iii*, cyclo-W(*d*)W. (d) Fluorescent lifetime and (e) fluorescent emission photostability of the crystals shown in (c). (f) Optical waveguiding of cyclo-FW crystals. Bright-field optical image (upper panel) and photoluminescent images (lower panels) of a single peptide platelet showing the waveguide upon laser excitation at different positions. The blue circles indicate the laser excitation; the red circles at the two edges show the outcoupled light. The width of the circles indicates the light intensity.

Europe PMC Funders Author Manuscripts

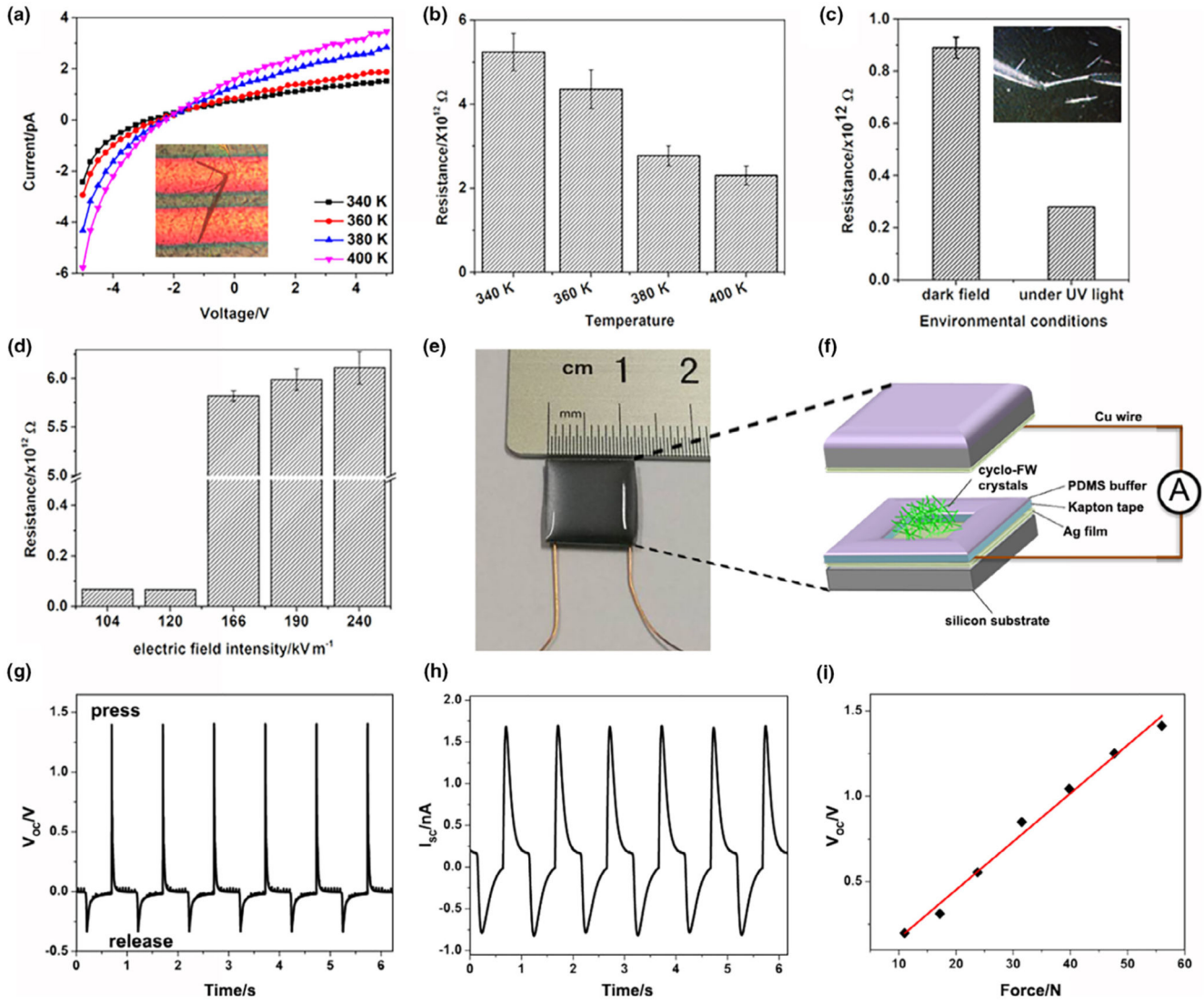

Figure 4. Electrical properties of the cyclo-FW crystals.

(a) Voltage–current curves of cyclo-FW crystals at different temperatures. (b) Statistical distribution of cyclo-FW crystals resistance at the temperatures shown in (a). (c) Conductivity characterization of cyclo-FW crystals in the dark or under UV light irradiation (256 nm). (d) Conductivity characterization of cyclo-FW crystals in different external electric fields. (e) Photograph of the generator utilized as a direct power source using cyclo-FW crystals as active components. (f) Schematic configuration of the peptide-based generator shown in (e). (g) Open-circuit voltage and (h) short-circuit current from the generator shown in (e). (i) Linear dependence of the open-circuit voltage on the applied forces. The insets in (a) and (c) show photographic pictures of the experimental measuring setups for (a, b) and (c, d), respectively.

Europe PMC Funders Author Manuscripts